Catalysis Letters (2020) 150:3424–3436
https://doi.org/10.1007/s10562-020-03257-1

Production of Hydrogen by Steam Reforming of Ethanol over Pd-Promoted Ni/SiO_2 Catalyst

Carlos Alberto Chagas[1] · Robinson Luciano Manfro[1] · Fabio Souza Toniolo[2]

Received: 9 March 2020 / Accepted: 7 May 2020 / Published online: 15 May 2020

Abstract

This study investigated the influence of palladium on the catalytic performance of Ni/SiO_2 obtained by incipient wetness impregnation method. Ni/SiO_2 and Pd–Ni/SiO_2 catalysts were tested in the steam reforming of ethanol for hydrogen production. X-ray diffraction, X-ray fluorescence spectroscopy, N_2 adsorption–desorption, temperature programmed reduction with hydrogen (H_2-TPR) and X-ray photoelectron spectroscopy were used to characterize the catalysts in detail. The incorporation of small amount of palladium into Ni/SiO_2 catalyst shifts the reduction of Ni species towards lower temperatures. All catalysts displayed total ethanol conversion and high H_2 selectivity (~ 60%) above 500 °C. Compared to other Ni-based catalysts reported in the recent literature, the catalysts here investigated show promising potential for further application in the hydrogen production by ethanol steam reforming, but CO selectivity should be decreased for fuel cell applications.

Graphic Abstract

Production of hydrogen by steam reforming of ethanol over Pd-promoted Ni/SiO_2 catalyst

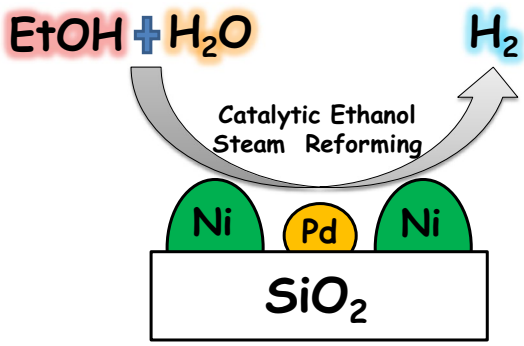

Keywords Nickel · Palladium · Promoters · Hydrogen · Ethanol

1 Introduction

Ethanol steam reforming (ESR) reaction ($C_2H_5OH + 3H_2O \rightarrow 6H_2 + 2CO_2$) using an appropriate catalyst is an efficient route for renewable hydrogen production and has been highlighted in the literature [1–6]. In addition, ethanol is atmospheric carbon neutral since the amount of CO_2 produced by steam reforming is consumed by the biomass growth, and this offers a nearly closed carbon loop not contributing to the greenhouse gas emissions [7, 8]. The selection and development of a suitable catalyst for ESR is a

Electronic supplementary material The online version of this article (https://doi.org/10.1007/s10562-020-03257-1) contains supplementary material, which is available to authorized users.

✉ Fabio Souza Toniolo
toniolo@peq.coppe.ufrj.br

[1] School of Chemistry—Federal University of Rio de Janeiro, P.O. BOX 68542, Rio de Janeiro 21941-909, Brazil

[2] Chemical Engineering Program of COPPE—Federal University of Rio de Janeiro, P.O. BOX 68502, Rio de Janeiro 21941-914, Brazil

key aspect, once the catalyst must be stable, active, selective, and maximize hydrogen production while simultaneously avoiding the formation of byproducts (CO and CH_4). Coke formation is a major issue in the ESR, which may lead to a decrease in catalytic activity and selectivity towards hydrogen, as well as to catalyst deactivation, limiting the industrial application [9, 10]. Carbon formation on the catalyst surface may take place via several reactions, such as ethanol dehydration to ethylene, followed by polymerization to coke; the "Boudouard" reaction; and decomposition of hydrocarbons (methane and ethylene) [11, 12]. The extent of each reaction depends on both chosen catalyst and reaction conditions.

Noble metal catalysts, such as Rh, Ru, Pd and Pt, can effectively break C–C and C–H bonds with a relatively good stability, but the fluctuating price and high cost limit their large-scale application [13, 14]. On the other hand, catalysts containing transition metals, mainly Ni [15–17] and Co [18–20], have been largely investigated as active catalysts for ESR reaction and exhibited catalytic activities comparable to those based on noble metals. Ni-based catalysts have been widely employed on commercial scale in reforming processes for more than 40 years [1], especially due to the excellent capability for C–C and C–H bond cleavage and low cost compared to expensive noble metals [21, 22]. However, Ni-based catalysts deactivate by carbon deposition and aggregation of active Ni particles more severely than noble metal catalysts, shortening their lifetime in the ESR reactions [1, 23]. Preventing the deactivation of Ni catalysts still remains a major challenge.

To minimize coke deposition and metal sintering, several alternatives have been suggested such as the addition of small amount of noble metals [7, 24]. Generally, it is possible to enhance the resistance to coke deposition and to prevent nickel sintering by adding small amount of noble metal promoters [25, 26]. Palma et al. [27] concluded that addition of small amount of Pt and Rh improves the catalytic performance and coke resistance in the ethanol reforming.

Pereira et al. [28] studied the effect of introducing small loading of Rh and Ru into Co/SiO_2 catalysts for the autothermal reforming of ethanol, aiming a synergistic effect between Co and Rh or Ru. Authors concluded that the noble metal facilitates the reduction of cobalt under experimental conditions of oxidative steam reforming of ethanol due to the intimate contact between Co and the noble metal (Ru or Rh) phases in the silica-supported bimetallic systems. Doping supported transition metal catalysts with palladium has been presented as promising to enhance the reduction of Ni under mild conditions and to improve the air-resistibility of Ni originated from the stabilization effect of Pd [29, 30].

Here we studied the influence of palladium on the catalytic performance of Ni/SiO_2 in the ethanol steam reforming for hydrogen production. Ni/SiO_2 and Pd–Ni/SiO_2 catalysts were prepared by incipient wetness impregnation method and characterized systematically by different techniques (XRD, XRF, N_2 adsorption–desorption, H_2-TPR and XPS) in order to understand the structure–activity relationship.

2 Experimental

2.1 Catalysts Preparation

Ni/SiO_2 and Pd–Ni/SiO_2 catalysts were synthesized by incipient wetness impregnation method [31]. The nominal loading amount of Ni and Pd were 10 and 1 wt.%, respectively. Commercial SiO_2 gel powder (Sigma-Aldrich, 60–200 mesh) used as support was previously calcined at 650 °C for 6 h under heating rate of 5 °C/min in a muffle furnace. Nickel was impregnated on the silica support (1.001 cm^3/g pore volume, obtained by N_2 adsorption/desorption experiments) with an aqueous solution of nickel precursor salt $Ni(NO_3)_2.6H_2O$ Sigma-Aldrich. After impregnation, the sample was dried in muffle furnace at 110 °C overnight followed by calcinations in 2 steps: firstly at 350 °C for 3 h (heating rate of 2 °C/min) and then at 650 °C for 5 h (5 °C/min) under static atmosphere. 1%Pd-10%Ni/SiO_2 catalyst was prepared by sequential impregnation of palladium over Ni/SiO_2 catalyst using a palladium nitrate aqueous solution ($Pd(NO_3)_2$, 10 wt.% in 10 wt.% nitric acid, Sigma-Aldrich). Subsequently, the sample was dried and calcined similarly. This first calcination step was carried out in order to prevent nickel to redissolve in the palladium solution during the second impregnation step. All catalysts were crushed and sieved to obtain the fraction between 0.18 and 0.12 mm, and from now on 10%Ni/SiO_2 and 1%Pd-10%Ni/SiO_2 catalysts are denominated as NiSiO and PdNiSiO, respectively.

2.2 Catalysts Characterization

Chemical composition analysis was performed by X-ray fluorescence spectroscopy (XRF) using a Rigaku spectrometer RIX 3100 model apparatus equipped with a rhodium standard tube as source of radiation. Around 300 mg of each sample was pelletized and analyzed quantitatively.

Textural properties were determined by nitrogen adsorption/desorption experiments at liquid nitrogen temperature using a Micromeritics ASAP2010 gas adsorption instrument. All samples were degassed under vacuum at 300 °C for 24 h prior to the measurements. The specific surface area was calculated using the Brunauer–Emmett–Teller (BET) method in a relative pressure range of 0.05–0.3. The pore size distribution was determined from desorption branches by the Barrett–Joyner–Halenda (BJH) method.

X-ray powder diffraction (XRD) measurements were performed in a Miniflex Rigaku diffractometer. The XRD patterns were collected using CuK_α radiation ($\lambda = 1.5406$

Å) operated at 30 kV and 15 mA in the range from 10 to 80° with a step size of 0.05° and counting time of 1 s per step. Crystalline phases were identified by using JCPDS (Joint Committee on Powder Diffraction Standards) database. The mean crystallite size was calculated using Scherrer equation. XRD patterns of the catalysts reduced ex-situ at the same conditions employed prior to the catalytic tests (*i.e.*, 600 °C for 2 h under 50 mL/min of H_2) were also obtained in order to analyze crystallographic features of the materials resulting from the activation pretreatment.

Temperature-programmed reduction with hydrogen (H_2-TPR) experiments were performed on a system equipped with a TCD detector employing a mixture of 1.53 vol.% H_2/Ar (30 mL/min) flowing through the sample. Prior to H_2-TPR analysis, the samples were pretreated at 150 °C for 30 min under argon flow of 30 mL/min and then cooled down to room temperature in argon gas flow before reduction. The temperature was linearly raised up to 1000 °C at 10 °C/min, and hydrogen consumption was continuously monitored by thermal conductivity detector (TCD). A trap of molecular sieve ensured the water retention prior to the detector, so that only hydrogen consumption was measured.

X-ray photoelectron spectroscopy (XPS) was performed to determine the chemical state and the surface composition of the calcined catalysts. XPS analysis was carried out using an ESCALAB 250 spectrometer (Thermo Scientific), employing monochromatic Al K_α (1486.6 eV) as X-ray source. The C 1 s signal at 284.6 eV was binding energy reference. Spectra were analyzed using a Gaussian-Lorenzian peak shape obtained from CasaXPS® software version 2.3.15.

Coke deposition on spent catalysts was determined by thermogravimetric analysis (TGA). Each sample was heated from room temperature (10 °C/min) up to 1000 °C under flow of air (60 mL/min). Quantification of coke was calculated according to the equation:

$$C = \frac{m_{coke}}{m_{usedcatalyst}\, x\, t}$$

In which m_{coke} is the mass of coke on the catalyst calculated from TGA profile; $m_{usedcatalyst}$ is the mass of catalyst remaining after TGA analysis, and t is the time-on-stream.

2.3 Catalytic Performance Test

The reforming reaction at stoichiometric conditions was conducted in a continuous fixed-bed quartz reactor at atmospheric pressure, and temperature from 200 up to 600 °C in steps of 100 °C. Initially, 200 mg of catalyst diluted with 400 mg of carborundum (SiC) was reduced in situ at 600 °C for 2 h flowing pure H_2 (50 mL/min) and then cooled down to room temperature under He flow (50 mL/min). This reduction conditions was established based on H_2-TPR analysis. Reactant mixture with H_2O/ethanol molar ratio = 3/1 was injected with a syringe pump (0.05 mL/min) into a vaporizer at 200 °C and mixed with a nitrogen flow (50 mL/min) before entering the reactor. The gas hourly space velocity (GHSV) of ethanol and water was 48,500 h^{-1}. Gaseous products were analyzed on line by gas chromatography (Shimadzu, model GC-2014) containing two columns (RT-QPLOT and Carboxen 1010) and equipped with a TCD using He as a carrier gas. The liquid phase was collected in the condensers and subsequently analyzed by a Shimadzu Prominence high-performance liquid chromatography (HPLC) equipped with a Bio-Rad Aminex HPX-87H column, using 0.01 M H_2SO_4 as eluent at 0.6 mL/min, and with UV and refractive index detectors. Time-on-stream stability tests were carried out at 500 °C in order to estimate deactivation of the catalysts. Ethanol conversion and selectivity to different gaseous products were calculated according to the equation used by Mondal et al. [7]. All the catalytic tests were carried out in duplicates and the values obtained for ethanol conversion showed a standard deviation below 3.0%.

Ethanol equilibrium conversion as a function of temperature was calculated taking into account the law of mass action described by Soave–Redlich–Kwong equation of state, and the equilibrium constant derived from the standard Gibbs free energy for the ESR reaction. According to thermodynamics analysis, ethanol equilibrium conversion is approximately total over the entire temperature range tested in this work (see Figure S1 in supplementary information, SI).

3 Results and Discussion

Table 1 shows results of textural and physicochemical properties of the catalysts and SiO_2 support. The chemical compositions measured by XRF revealed that Ni and Pd contents are in good agreement with nominal composition, indicating that the synthesis method was appropriate to incorporate the metal loading.

The nitrogen adsorption/desorption measurements and the Barrett Joyner Halenda (BJH) pore size distributions are shown in Fig. 1. All isotherms are similar to type IV according to the IUPAC classification, indicating the mesoporous nature of the materials [32]. In all the cases it was found a narrow pore size range with mean diameter about 100 Å, as evidenced in the BJH pore size distribution profiles (Fig. 1). Textural properties (surface area, pore volume, mean pore diameter) of the SiO_2 support and catalysts obtained from the adsorption–desorption isotherms of nitrogen are also summarized in Table 1. BET surface area and pore volume of SiO_2 support decreased after incorporation of the metals (Ni and Pd), which can be attributed to the partial plugging

Table 1 Physicochemical and textural properties of the catalysts and SiO_2 support

Catalyst	Chemical composition (wt.%)			S_{BET} (m^2/g)	V_{pore} (cm^3/g)	D_{BJH} (Å)	L_c*(Å)	
	Pd	Ni	SiO_2				PdO	NiO
SiO_2 (support)	–	–	100	284	1.001	110	–	–
NiSiO	–	9.3	90.7	258	0.863	110	–	140
PdNiSiO	1.1	9.5	89.4	200	0.773	103	80	145

S_{BET} specific surface area obtained from BET method; V_{pore} Derived from single point measured at P/P_0 = 0.98; D_{BJH} desorption mean pore diameter

*Mean crystallite size calculated by Scherrer equation

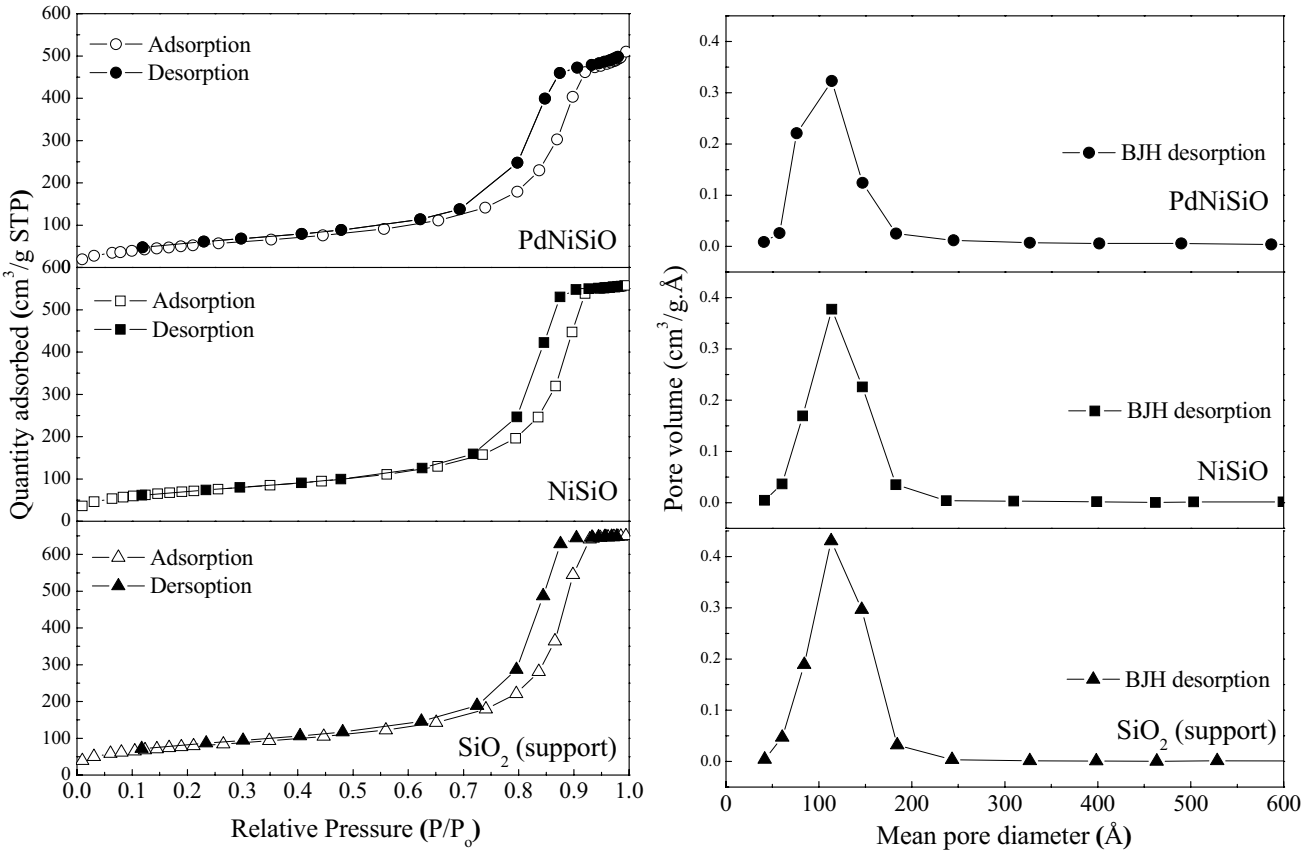

Fig. 1 N_2 adsorption–desorption isotherms and pore size distribution of the catalysts and SiO_2 support

of SiO_2 mesopores by NiO and PdO crystals limiting the accessibility of N_2 molecules.

The successful syntheses of the catalysts were also confirmed by X-ray diffraction (XRD) patterns in Fig. 2. All XRD patterns presented a diffuse peak around 2θ = 23°, corresponding to (101) diffraction plane, which agrees with that expected for α-cristobalite silica (JCPDS n°. 39–1425). The XRD patterns of NiSiO and PdNiSiO catalysts exhibited the diffraction peak relative to silica, and additional peaks at 2θ = 37, 43 and 62°. These peaks correspond to (111), (200) and (220) diffraction planes related to NiO phase (JCPDS no. 41-1107). This result also suggests that the Pd addition did not modify the nature of the nickel phase. Importantly, a small peak located at 2θ = 34.2° in the XRD pattern of PdNiSiO catalyst corresponding to (101) diffraction plane can be attributed to PdO phase (JCPDS no. 41-1107). The mean crystallite sizes for PdO and NiO were estimated by using the Scherrer equation and the values are given in Table 1. Therefore, the second calcination after addition of palladium did not affect the dimension of NiO crystallites. The catalysts were reduced ex-situ at the same conditions employed prior to the catalytic tests and were immediately analyzed by XRD. Diffractograms are displayed in Fig. S2 (SI) and we verified absence of diffraction peaks for metallic palladium

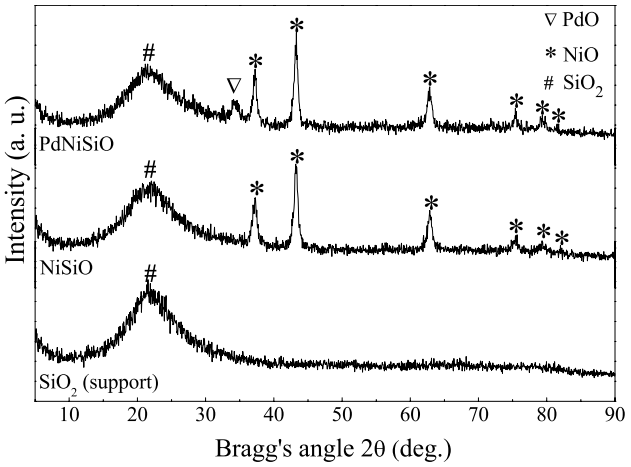

Fig. 2 XRD patterns of the calcined catalysts and SiO_2 support

phases for both NiSiO and PdNiSiO. This finding suggests that Pd^0 is highly dispersed on SiO_2 surface. On the other hand, metallic Ni phase (JCPDS no. 65-2865) was identified with mean crystallite size of 195 and 167 Å for NiSiO and PdNiSiO catalysts, respectively (i.e., smaller for the bimetallic catalyst). Therefore, these mean coherent domain sizes suggest an estimate of Ni dispersion higher on the bimetallic catalyst after reduction.

H_2-TPR experiments were performed to determine the appropriate reduction temperature to activate the catalysts prior the tests, as well as to infer about the chemical interaction between metals (Ni and Pd) and SiO_2 support. The reduction profiles of the catalysts and SiO_2 support are depicted in Fig. 4. All of the catalysts exhibited a H_2-TPR profile similar and relatively complex formed by two consecutive temperature regions. The reduction peaks in the low temperature range (around 300–600 °C) can be attributed to the reduction of Ni species ($NiO \rightarrow Ni^0$), which are free nickel oxide species and have a weak interaction with the silica support; whereas the reduction peaks in the high temperature range (620–900 °C) corresponds to a stronger interaction of NiO species with support [33, 34]. This result is in good agreement with literature [35–40] and clearly demonstrate different degrees of interaction between NiO species and SiO_2 support. For PdNiSiO catalyst, a small reduction peak at lower temperature (about 95 °C) can be assigned to the reduction of PdO (detected previously by XRD measurement) to metallic Pd [41, 42]. In addition, we detected a significant consumption of hydrogen at room temperature for PdNiSiO catalyst. It is well known that the reduction of PdO normally takes place at room temperature [43–45], therefore the peak at 95 °C suggests some PdO having some stronger interaction with nickel and/or SiO_2. Our results indicate that PdO species reduces predominantly at room temperature, but some fraction of PdO reduces at 95 °C.

In the case of PdNiSiO catalyst, the main peak for NiO reduction (350–600 °C) is larger than the corresponding one for NiSiO, as depicted in Fig. 3. That happens because part of NiO species that reduces at high temperature on NiSiO (600–850 °C) shifts to lower temperature on PdNiSiO (at the range of 500–600 °C roughly). Therefore, by adding Pd on NiSiO a fraction of NiO is more easily reduced, concentrating this reduction at the range of 350–600 °C (and not at 350–800 °C as observed for NiSiO). According to several studies reported in literature [8, 42, 46–48] this occurs because palladium catalyzes the reduction of Ni species (with strong and weak interaction with support) by shifting the Ni^{2+} peak towards lower temperatures as a result of H_2 spillover process.

Quantitative analysis of H_2-TPR profiles revealed a high reduction degree for nickel and palladium species on all the catalysts, as shown in Table 2 by comparing the theoretical and experimental H_2 uptake to reduce NiO and PdO species into Ni and Pd, respectively. The total amount of consumed

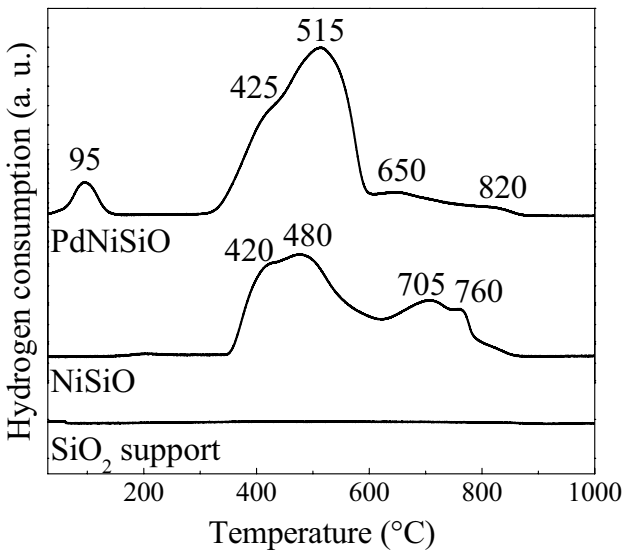

Fig. 3 H_2-TPR profiles of the calcined catalysts and SiO_2 support

Table 2 Quantitative results for H_2-TPR analysis

Catalyst	H_2 consumption (μmol)		Reduction degree (%)	
	NiO[a]	PdO[b]	Ni	Pd
NiSiO	228 (245)[c]	–	93	–
PdNiSiO	264 (288)[c]	19 (19)[c]	92	100

[a]Assuming that all nickel is present as NiO (as confirmed by XRD measurements)

[b]Assuming that all palladium is present as PdO (as obtained by XRD measurements)

[c]Theoretical consumption of hydrogen

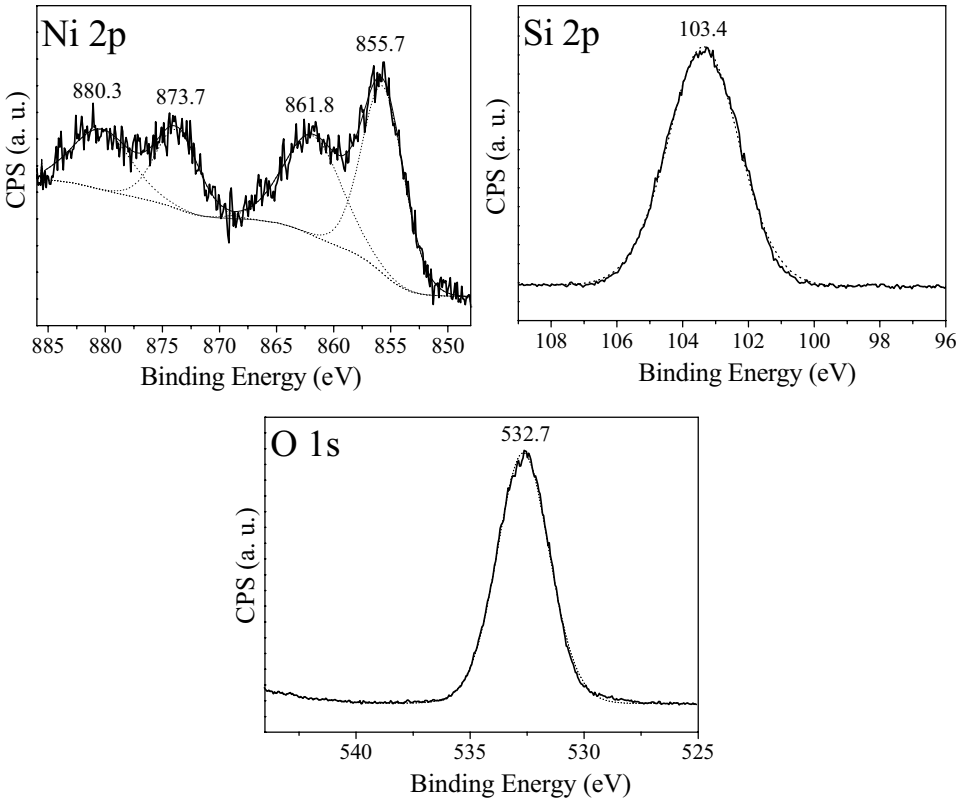

Fig. 4 XP spectra of the calcined NiSiO catalyst

hydrogen was similar for both catalysts, indicating that the reduction degree was independent from the presence of palladium. The noble metal increased the ability of NiO to reduce at lower temperature but did not affect the reduction degree. The total H_2 consumption by PdO species (19 µmol) was calculated by the combined reduction of Pd^{2+} species at room temperature and species having a stronger interaction with the support at 95 °C, and it was equivalent to the theoretical requirement for complete reduction of PdO species taking into account the real loading of Pd as provided by XRF analysis (Table 1).

The surface species were investigated by XPS analysis and the XP spectra of Ni 2p, Si 2p and O 1 s regions for NiSiO are depicted in Fig. 4. Peaks related to impurities were not detected. The spectrum relative to nickel exhibited two peaks around 855.7 and 861 eV corresponding to Ni $2p_{3/2}$ line, followed by two relatively intense peaks at 873.7 and 880.3 eV which are associated to Ni $2p_{1/2}$ line. These binding energies are indicative of the existence of Ni species in the form of bivalent state as NiO [48]. The Si 2p and O 1 s binding energies were found to be 103.4 and 532.7 eV, respectively, characteristic of silicon dioxide [49]. These findings indicate a similar oxidation state of the elements on surface and in the bulk, as evidenced previously by XRD analysis (Fig. 1).

The XP spectra of the bimetallic PdNiSiO catalyst are presented in Fig. 5. The spectrum of palladium can be deconvoluted into two pairs of doublets. The doublet centered at 338.1 and 344.0 eV correspond to Pd^{2+} species [50], confirming that palladium exists on the surface as PdO. Conversely, the doublet located at 336.6 and 342.1 eV agrees with those reported for metallic Pd (Pd^0). This finding can be attributed to the reduction of PdO species during XPS measurements probably resulting from exposing the sample to the X-ray beam.

The Ni 2p region was decomposed into four contributions typical of Ni^{2+} species in the NiO form, similar to NiSiO catalyst (Fig. 4). The spectrum relative to the Si 2p region can be fitted to two peaks at 102.8 and 104.6 eV. The first peak is associated to the silicon atom bonded to hydroxyl group (Si–OH), while the second one is related to -O-Si–O- on the surface silicon dioxide [51, 52]. The spectrum of O 1 s showed two components centered at 532.1 and 533.8 eV which are associated to Si–O-Si and Si–O-H bonds, respectively [53, 54].

3.1 Evaluation of Catalysts Performance

The catalytic activity in the ESR reaction was evaluated at the temperature range of 300–600 °C. Ethanol conversion and product distribution for both NiSiO and PdNiSiO catalysts are presented in Figs. 6 and 7, respectively. On all catalysts, the conversion of ethanol increased significantly as a function of the reaction temperature, reflecting the

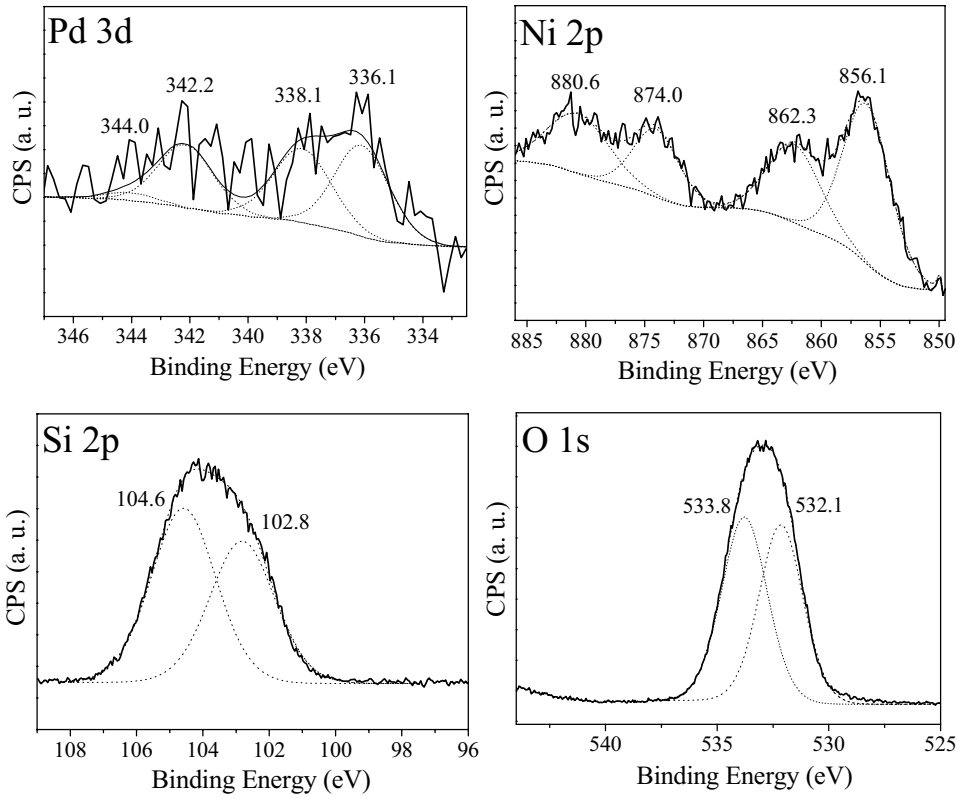

Fig. 5 XP spectra of the calcined PdNiSiO catalys

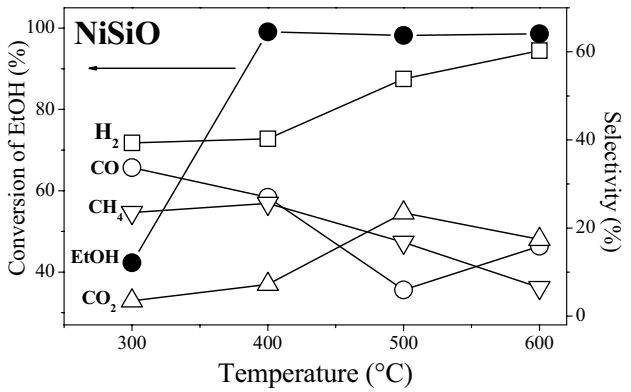

Fig. 6 Effect of temperature on ethanol conversion (filled symbols) and product selectivity (empty symbols) over NiSiO catalyst

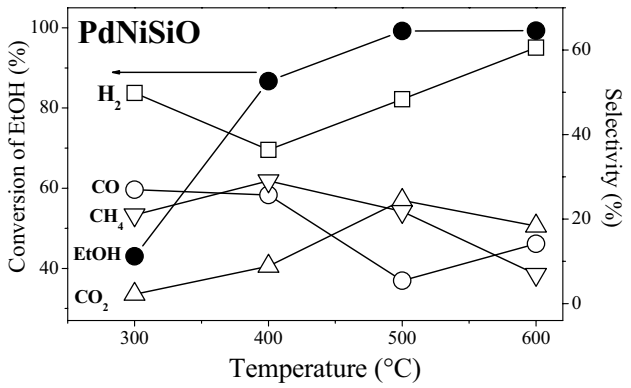

Fig. 7 Effect of temperature on ethanol conversion (filled symbols) and product selectivity (empty symbols) over PdNiSiO catalyst

endothermic feature of the reforming reaction. For NiSiO catalyst, the total conversion of ethanol was obtained from 400 °C. On the other hand, PdNiSiO catalyst led to total ethanol conversion from 500 °C. At the temperature range of 300–600 °C the equilibrium conversion of ethanol is ≥ 99.6% (Figure S1 in Supplementary Information), therefore a more suitable comparison of NiSiO and PdNiSiO can be done at 300 and 400 ºC. Both NiSiO and PdNiSiO presented similar ethanol conversion at 300ºC (≈42%), but the bimetallic catalyst showed higher H_2 selectivity (≈50%) than the monometallic one (≈40%). At 400ºC, NiSiO shows higher activity than PdNiSiO ($X_{EtOH} = 100\%$ *vs* 90%, respectively), and only at 500ºC the bimetallic material reaches the same activity of NiSiO for ethanol conversion (≈100%). The bimetallic PdNiSiO seems to be slightly less active than NiSiO at low temperatures, but more selective to H_2. Moreover, the rates of coke formation calculated after 30 h on stream indicate that the bimetallic PdNiSiO is less prone to deactivation, as will be discussed afterwards.

Regarding product distribution, the main products formed over the catalysts were H_2, CO, CO_2 and CH_4. With respect to H_2 production, PdNiSiO catalyst exhibited an initial H_2

selectivity of 50% at 300 °C, while the initial H_2 selectivity obtained over the NiSiO catalyst was 40% under the same ethanol isoconversion condition (approx. 42%). This result suggests that the addition of palladium have positive effects on the initial H_2 selectivity at lower temperature (300 °C) and can be attributed to the ability of Pd to promote steam reforming and water gas shift reaction, and to suppress coke formation reactions [7]. However, the maximum H_2 selectivity was equal for both catalysts (S_{H2} = 60%) and was obtained at 600 °C. For NiSiO catalyst, CO and CH_4 selectivities slightly decreased by increasing temperature from 400 to 500 °C, while selectivity to H_2 and CO_2 enhanced, suggesting that water gas shift reaction ($CO + H_2O \rightarrow CO_2 + H_2$) and methane steam reforming ($CH_4 + H_2O \rightarrow CO + 3H_2$) were favored. Methanation and WGS reaction are the main parallel side reactions in the ESR, and significantly affect the product distribution [55]. Similar behavior was observed over PdNiSiO catalyst.

Above 500 °C, both catalysts exhibited an increase in CO selectivity, while the CO_2 concentration diminished, implying in the reverse water gas shift reaction ($CO_2 + H_2 \rightarrow CO + H_2O$) [56]. Interestingly, for PdNiSiO catalyst one can observe a decrease in the selectivity to H_2 and CO when the temperature increases from 300 to 400 °C. That can be attributed to the methanation reaction ($CO + 3H_2 \rightarrow CH_4 + H_2O$) [57], for which both H_2 and CO are converted into CH_4, which is a coproduct experimentally quantified at that temperature range. Methanation is an endothermic reaction and thus is favored by the high temperature. The presence of intermediate products (acetaldehyde or ethylene) was not detected in the product stream at the range of temperature studied. This result is in agreement with previous studies which evidenced that temperatures in the range of 450–600 °C led to higher ethanol conversion and H_2 selectivity [58–61].

It was expected that loading palladium in the NiSiO catalyst could increase both ethanol conversion and selectivity to H_2 in the product stream. However, this promotion effect was not observed over all temperature range studied. On the other hand, the incorporation of Pd into NiSiO catalyst caused a significant increase in the initial H_2 selectivity and decrease in the concentrations of CO in the gaseous products at 300 °C. This result can be attributed to the presence of well-dispersed palladium species which are responsible for facilitating the reduction of nickel oxide species and shifting its reduction to lower temperatures, and thus enhancing the chemical activity of Pd-promoted NiSiO catalyst. This hypothesis is supported by XRD and H_2-TPR analysis, as discussed previously.

In order to verify the relevance of NiSiO and PdNiSiO catalysts, their performance was compared to previous studies over similar nickel-based catalysts in the ESR reaction (see Table 3). The differences in the results can be explained by the nature of the catalysts and also the different operating conditions. Comparing our results to those reported in the recent literature (Table 3), most of findings indicate selectivity to H_2 in between 48 and 70%, and our results fit into this range. However, concerning the selectivity to CO, NiSiO and PdNiSiO lead to lower values (5.5–6.0%) than most of reported studies (9–30%), which is interesting once low concentration of CO is desired. We can conclude that supported-Ni promoted catalyst are suitable materials for hydrogen production by ethanol steam reforming, but that CO selectivity should be reduced for fuel cell applications.

3.2 Stability Test

The ESR is considered as a harsh reaction, generally causing serious catalyst deactivation after a long-term operation. Therefore, stability is a key issue in the development of catalysts for H_2 production by ESR. This work evaluated the stability of the catalysts during 30 h on stream at 500 °C. Figure 8 shows ethanol conversion and selectivity to compounds (H_2, CO, CO_2 and CH_4) as a function of time for NiSiO and PdNiSiO catalysts. Both materials presented ethanol conversion of 100% during 30 h on stream. H_2 selectivity decreased significantly after 8 h for NiSiO and PdNiSiO; on the other hand, CO and CO_2 selectivities remained approximately constant and CH_4 selectivity slightly increased as a function of time. These results are attributed to the occurrence of methanation reaction which is favored at high temperatures. After 8 h on stream, the product distribution remained quite constant until 30 h. The results clearly demonstrate a similar stability for both catalysts in the ESR reaction.

The catalyst deactivation during the ESR process is mainly caused by carbon deposition. To check the deactivation, the spent catalysts (after 30 h on stream) were characterized by TGA analysis and the profiles are illustrated in Fig S3 (SI). For both NiSiO and PdNiSiO catalysts the weight loss occurred at the range of 550–650 °C, which can be attributed to the combustion of graphitic/filamentous coke on the catalyst surface [68]. Saturated C–C bond such as paraffinic or amorphous carbon tends to oxidize at lower temperatures ($T_{oxidation}$ = 400–550 °C) than unsaturated hydrocarbon such as olefins, graphitic and filamentous carbon ($T_{oxidation}$ = 550–650 °C). As reported in literature, the carbon deposited on the catalyst surface during ESR reaction can have amorphous or filamentous nature [69]. Amorphous carbon leads to a more severe deactivation if compared to filamentous carbon [66]. In this investigation, both NiSiO and PdNiSiO catalysts were stable after 30 h on stream and presented some coke formation which was quantified in terms of $mg_{coke}\ g_{cat}^{-1}\ h^{-1}$ (as detailed in the sequence). Also, TGA results of the spent catalysts suggested a filamentous nature of the coke as previously discussed. Such carbon does not block Ni^0 active

Table 3 Results reported in literature for ethanol conversion and hydrogen selectivity over various catalysts, and NiSiO and PdNiSiO of this present study

Catalytic system	Operating conditions in ESR	X_{EtOH} (%)	Main products (selectivity)	References
$1\%Ni/Ce_{0.9}Sm_{0.1}O_{2-\delta}$	Catalyst weight = 100 mg Reaction temperature = 550 °C Atmospheric pressure H_2O/EtOH molar ratio = 3 GHSV = 6,115 h^{-1}	100	H_2 (55%), CO (30%), CO_2 (45%) and CH_4 (15%)	[61]
$10\%Ni@CeO_2$	Catalyst weight = 100 mg Reaction temperature = 600 °C Atmospheric pressure H_2O/EtOH molar ratio = 3 GHSV = 12,000 h^{-1}	70	H_2 (55%), CO (12%), CO_2 (5%) and CH_4 (10%)	[62]
$0.25\%Rh\text{-}10\%Ni/La_2O_3\text{-}CeO_2\text{-}Al_2O_3$	Catalyst weight = 100 mg Reaction temperature = 500 °C Atmospheric pressure H_2O/EtOH molar ratio = 3 GHSV = 26,000 h^{-1}	100	H_2 (68%), CO (4.5%), CO_2 (14%) and CH_4 (13%)	[15]
$7\%Ni/CeO_2MgO$	Catalyst weight = 30 mg Reaction temperature = 600 °C Atmospheric pressure H_2O/EtOH molar ratio = 3 GHSV = 5,000 h^{-1}	100	H_2 (70%), CO (9%), CO_2 (20%) and CH_4 (4%)	[63]
$15\%Ni/La_2O_3\text{-}CeO_2\text{-}Al_2O_3$	Catalyst weight = 100 mg Reaction temperature = 650 °C Atmospheric pressure H_2O/EtOH molar ratio = 3 GHSV = 27,000 h^{-1}	100	H_2 (58%), CO (25%), CO_2 (13%) and CH_4 (5%)	[64]
3%Pt/10%Ni/CeZr	Catalyst weight = 548 mg Reaction temperature = 500 °C Atmospheric pressure H_2O/EtOH molar ratio = 3 GHSV = 114,350 h^{-1}	100	H_2 (49%), CO (16%), CO_2 (51%) and CH_4 (33%)	[65]
$LaNiO_3$	Catalyst weight = 75 mg Reaction temperature = 700 °C Atmospheric pressure H_2O/EtOH molar ratio = 3 GHSV = 60,000 h^{-1}	100	H_2 (60%), CO (25%), CO_2 (15%) and CH_4 (3%)	[66]
$LaCo_{0.3}Ni_{0.7}O_3$	Catalyst weight = 75 mg Reaction temperature = 700 °C Atmospheric pressure H_2O/EtOH molar ratio = 3 GHSV = 120,000 h^{-1}	100	H_2 (60%), CO (25%), CO_2 (15%) and CH_4 (3%)	[66]
$10\%Ni/CeO_2$	Catalyst weight = 150 mg Reaction temperature = 550 °C Atmospheric pressure H_2O/EtOH molar ratio = 3 GHSV = 40,000 h^{-1}	100	H_2 (61%), CO (12%), CO_2 (19%) and CH_4 (7%)	[67]
$10\%Ni/SiO_2$	Catalyst weight = 200 mg Reaction temperature = 500 °C Atmospheric pressure H_2O/EtOH molar ratio = 3 GHSV = 48,500 h^{-1}	100	H_2 (54%), CO (6%), CO_2 (23%) and CH_4 (17%)	**This work**
$1\%Pd\text{-}10\%Ni/SiO_2$	Catalyst weight = 200 mg Reaction temperature = 500 °C Atmospheric pressure H_2O/EtOH molar ratio = 3 GHSV = 48,500 h^{-1}	100	H_2 (48%), CO (5.5%), CO_2 (24%) and CH_4 (22%)	

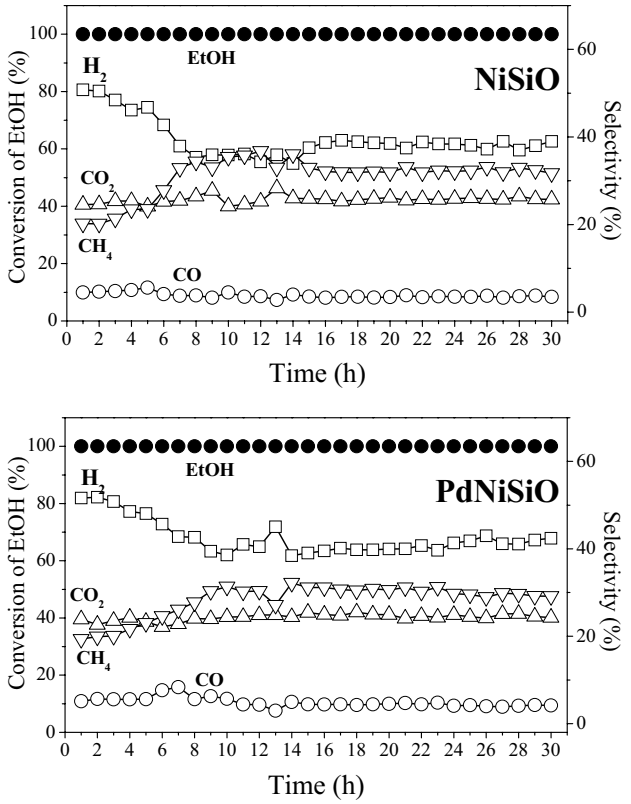

Fig. 8 Time-on-stream stability results for NiSiO catalyst (upper) and PdNiSiO (down) at 500 °C for 30 h in the ethanol steam reforming

sites, and for this reason the catalytic activity remains constant (Fig. 8). However, excessive carbon accumulation may result in plugging of the reactor and pressure drop, which was not observed after 30 h on stream at the experimental conditions. Therefore, we suggest that the possible route for coke formation on NiSiO and PdNiSiO has been derived from Boudouard reaction ($2CO \rightarrow CO_2 + C$) and methane decomposition ($CH_4 \rightarrow C + 2H_2$).

The coke formation rates were calculated from TGA profiles and results are summarized in Table 4. We verified that coke deposition on NiSiO catalyst (1.41 $mg_{coke}\ g_{cat}^{-1}\ h^{-1}$) was higher than on PdNiSiO (1.13 $mg_{coke}\ g_{cat}^{-1} h^{-1}$), suggesting that addition of Pd suppresses coke formation. This result is in good accordance with previous works [8, 69, 70] showing that noble metals are more resistant to carbon formation than non noble metals. Table 4 allows a comparison between our results and other Ni-based catalysts reported in the recent literature [9, 71–75] under similar reaction conditions. PdNiSiO and NiSiO exhibited improved resistance to coke deposition, once catalysts reported in literature showed coke formation rates of one or even two orders of magnitude higher than reported in the present study. These results suggest that the catalysts developed in this work are promising and competitive candidate for ESR reaction.

Table 4 Carbon formation rates during time-on-stream stability tests in the ethanol steam reforming. Data from literature are shown for comparison

Catalyst	Reaction conditions (Coke formation rate)	Reference
10%Ni/SiO_2	S/C = 3; GHSV = 48,500 h^{-1} (1.41 $mg_{coke}\ g_{cat}^{-1}\ h^{-1}$)	**This work**
1%Pd-10%Ni/SiO_2	S/C = 3; GHSV = 48,500 h^{-1} (1.13 $mg_{coke}\ g_{cat}^{-1}\ h^{-1}$)	
18%NiO/αAl_2O_3	S/C = 3; GHSV = 400–800 h^{-1} (4.7 $mg_{coke}\ g_{cat}^{-1}\ h^{-1}$)	[71]
15%Ni/Al_2O_3-La_2O_3	S/C = 3; GHSV = 23,140 mL/g h (16.3 $mg_{coke}\ g_{cat}^{-1}\ h^{-1}$)	[72]
15%Ni/La-Sn–O	S/C = 4.5; GHSV = 41,000 h^{-1} (7.8 $mg_{coke}\ g_{cat}^{-1}\ h^{-1}$)	[73]
10%Ni/SiO_2	S/C = 3; $WHSV_{EtOH}$ = 10 h^{-1} (169 $mg_{coke}\ g_{cat}^{-1}\ h^{-1}$)	[9]
$LaNi_{0.85}Zn_{0.15}O_{3-\delta}$	S/C = 3; WHSV = 18.4 h^{-1} (19.9 $mg_{coke}\ g_{cat}^{-1}\ h^{-1}$ during 8 h; 2.0 $mg_{coke}\ g_{cat}^{-1}\ h^{-1}$ during 100 h)	[74]
8%Ni/Ce-$MgAl_2O_4$	S/C = 3; W/F_{EtOH} = 0.81 g h/mol (23 $mg_{coke}\ g_{cat}^{-1}\ h^{-1}$)	[75]

4 Conclusions

In this study, Ni/SiO_2 catalyst promoted with small amount of palladium was successfully synthesized by incipient wetness impregnation method and tested in the steam reforming of ethanol for hydrogen production. Palladium catalyzed the reduction of Ni species interacting strongly with the silica support. All catalysts displayed total ethanol conversion and high H_2 selectivity (~60%) above 500 °C. The characterization results of the spent catalysts revealed that the loss of activity after 8 h on stream for both catalysts is due to the formation of filamentous/graphitic carbon. The Pd-promoted catalyst exhibited higher resistance to coke deposition and higher stability in comparison with the unpromoted material. Comparing our results with those reported in the recent literature, we can conclude that Ni/SiO_2 and Pd–Ni/SiO_2 catalysts are suitable materials for hydrogen production by ethanol steam reforming reaction, but CO selectivity should be decreased for fuel cell applications.

Acknowledgements The authors gratefully thank CNPq (Conselho Nacional de Desenvolvimento Científico) and FAPERJ (Fundação de Amparo à Pesquisa do Estado do Rio de Janeiro) for financial support; RECAT/UFF (Laboratório de Cinética, Catálise e Reatores Químicos da Universidade Federal Fluminense) for XPS analysis; and Jeiveison G.S.S. Maia for the thermodynamics calculations.

References

1. Sehested J (2006) Four challenges for nickel steam-reforming catalysts. Catal Today 111:103–110. https://doi.org/10.1016/j.cattod.2005.10.002
2. Breen JP, Burch R, Coleman HM (2002) Metal-catalysed steam reforming of ethanol in the production of hydrogen for fuel cell applications. Appl Catal B Environ 39:65–74. https://doi.org/10.1016/S0926-3373(02)00075-9
3. Goula MA, Kontou SK, Tsiakaras PE (2004) Hydrogen production by ethanol steam reforming over a commercial Pd/γ-Al_2O_3 catalyst. Appl Catal B Environ 49:135–144. https://doi.org/10.1016/j.apcatb.2003.12.001
4. Vaidya PD, Rodrigues AE (2006) Insight into steam reforming of ethanol to produce hydrogen for fuel cells. Chem Eng J 117:39–49. https://doi.org/10.1016/j.cej.2005.12.008
5. Fatsikostas AN, Verykios XE (2004) Reaction network of steam reforming of ethanol over Ni-based catalysts. J Catal 225:439–452. https://doi.org/10.1016/j.jcat.2004.04.034
6. Navarro RM, Sánchez-Sánchez MC, Alvarez-Galvan MC et al (2009) Hydrogen production from renewable sources: Biomass and photocatalytic opportunities. Energy Environ Sci 2:35–54. https://doi.org/10.1039/b808138g
7. Mondal T, Pant KK, Dalai AK (2015) Catalytic oxidative steam reforming of bio-ethanol for hydrogen production over Rh promoted Ni/CeO2-ZrO2 catalyst. Int J Hydrog Energy 40:2529–2544. https://doi.org/10.1016/j.ijhydene.2014.12.070
8. Profeti LPR, Dias JAC, Assaf JM, Assaf EM (2009) Hydrogen production by steam reforming of ethanol over Ni-based catalysts promoted with noble metals. J Power Sour 190:525–533. https://doi.org/10.1016/j.jpowsour.2008.12.104
9. Zhurka MD, Lemonidou AA, Anderson JA, Kechagiopoulos PN (2018) Kinetic analysis of the steam reforming of ethanol over Ni/SiO2 for the elucidation of metal-dominated reaction pathways. React Chem Eng 3:883–897. https://doi.org/10.1039/c8re00145f
10. Vicente J, Ereña J, Montero C et al (2014) Reaction pathway for ethanol steam reforming on a Ni/SiO2 catalyst including coke formation. Int J Hydrog Energy 39:18820–18834. https://doi.org/10.1016/j.ijhydene.2014.09.073
11. Cavallaro S (2000) Ethanol steam reforming on Rh/Al_2O_3 Catalysts. Energy Fuels 14:1195–1199. https://doi.org/10.1021/ef0000779
12. Bilal M, Jackson SD (2012) Steam reforming of ethanol at medium pressure over Ru/Al2O 3: effect of temperature and catalyst deactivation. Catal Sci Technol 2:2043–2051. https://doi.org/10.1039/c2cy20267k
13. Carbajal-Ramos IA, Gomez MF, Condó AM et al (2016) Catalytic behavior of Ru supported on Ce0.8Zr0.2O2 for hydrogen production. Appl Catal B Environ 181:58–70. https://doi.org/10.1016/j.apcatb.2015.07.025
14. Moraes TS, Rabelo Neto RC, Ribeiro MC et al (2016) Ethanol conversion at low temperature over CeO_2-supported Ni-based catalysts. Effect of Pt addition to Ni catalyst. Appl Catal B Environ 181:754–768. https://doi.org/10.1016/j.apcatb.2015.08.044
15. Campos CH, Pecchi G, Fierro JLG, Osorio-Vargas P (2019) Enhanced bimetallic Rh-Ni supported catalysts on alumina doped with mixed lanthanum-cerium oxides for ethanol steam reforming. Mol Catal 469:87–97. https://doi.org/10.1016/j.mcat.2019.03.007
16. Szijjártó GP, Pászti Z, Sajó I et al (2013) Nature of the active sites in Ni/$MgAl_2O_4$-based catalysts designed for steam reforming of ethanol. J Catal 305:290–306. https://doi.org/10.1016/j.jcat.2013.05.036
17. Marinho ALA, Rabelo-Neto RC, Noronha FB, Mattos LV (2016) Steam reforming of ethanol over Ni-based catalysts obtained from $LaNiO_3$ and $LaNiO_3$/$CeSiO_2$ perovskite-type oxides for the production of hydrogen. Appl Catal A Gen 520:53–64. https://doi.org/10.1016/j.apcata.2016.03.032
18. Kubacka A, Fernández-García M, Martínez-Arias A (2016) Catalytic hydrogen production through WGS or steam reforming of alcohols over Cu, Ni and Co catalysts. Appl Catal A Gen 518:2–17. https://doi.org/10.1016/j.apcata.2016.01.027
19. Song H, Ozkan US (2009) Ethanol steam reforming over Co-based catalysts: role of oxygen mobility. J Catal 261:66–74. https://doi.org/10.1016/j.jcat.2008.11.006
20. Sohn H, Ozkan US (2016) Cobalt-based catalysts for ethanol steam reforming: an overview. Energy Fuels 30:5309–5322. https://doi.org/10.1021/acs.energyfuels.6b00577
21. Zhou G, Barrio L, Agnoli S et al (2010) High activity of Ce1-xNixO_2-y for H_2 production through ethanol steam reforming: Tuning catalytic performance through metal-oxide interactions. Angew Chemie Int Ed 49:9680–9684. https://doi.org/10.1002/anie.201004966
22. Pu J, Nishikado K, Wang N et al (2018) Core-shell nickel catalysts for the steam reforming of acetic acid. Appl Catal B Environ 224:69–79. https://doi.org/10.1016/j.apcatb.2017.09.058
23. Chen LC, Lin SD (2011) The ethanol steam reforming over Cu-Ni/SiO_2 catalysts: Effect of Cu/Ni ratio. Appl Catal B Environ 106:639–649. https://doi.org/10.1016/j.apcatb.2011.06.028
24. Kugai J, Subramani V, Song C et al (2006) Effects of nanocrystalline CeO_2 supports on the properties and performance of Ni-Rh bimetallic catalyst for oxidative steam reforming of ethanol. J Catal 238:430–440. https://doi.org/10.1016/j.jcat.2006.01.001
25. Parizotto NV, Rocha KO, Damyanova S et al (2007) Alumina-supported Ni catalysts modified with silver for the steam reforming of methane: effect of Ag on the control of coke formation. Appl Catal A Gen 330:12–22. https://doi.org/10.1016/j.apcata.2007.06.022
26. Vizcaíno AJ, Carrero A, Calles JA (2007) Hydrogen production by ethanol steam reforming over Cu-Ni supported catalysts. Int J Hydrog Energy 32:1450–1461. https://doi.org/10.1016/j.ijhydene.2006.10.024
27. Palma V, Ruocco C, Meloni E, Ricca A (2017) Influence of catalytic formulation and operative conditions on coke deposition over CeO_2-SiO_2 based catalysts for ethanol reforming. Energies 10:1030. https://doi.org/10.3390/en10071030
28. Pereira EB, Homs N, Martí S et al (2008) Oxidative steam-reforming of ethanol over Co/SiO_2, Co-Rh/SiO_2 and Co-Ru/SiO_2 catalysts: catalytic behavior and deactivation/regeneration processes. J Catal 257:206–214. https://doi.org/10.1016/j.jcat.2008.05.001
29. Ai F, Yao A, Huang W et al (2010) Synthesis of PVP-protected NiPd nanoalloys by modified polyol process and their magnetic properties. Phys E Low-Dimensional Syst Nanostruct 42:1281–1286. https://doi.org/10.1016/j.physe.2009.10.050
30. Lu P, Teranishi T, Asakura K et al (1999) Polymer-protected Ni/Pd bimetallic nano-clusters: preparation, characterization and catalysis for hydrogenation of nitrobenzene. J Phys Chem B 103:9673–9682. https://doi.org/10.1021/jp992177p
31. Lertwittayanon K, Atong D, Aungkavattana P et al (2010) Effect of CaO-ZrO_2 addition to Ni supported on γ-Al_2O_3 by sequential impregnation in steam methane reforming. Int J Hydrog Energy 35:12277–12285. https://doi.org/10.1016/j.ijhydene.2010.08.098
32. Leofanti G, Padovan M, Tozzola G, Venturelli B (1998) Surface area and pore texture of catalysts. Catal Today 41:207–219. https://doi.org/10.1016/S0920-5861(98)00050-9
33. Wang Y, Zhu A, Zhang Y et al (2008) Catalytic reduction of NO by CO over NiO/CeO_2 catalyst in stoichiometric NO/CO and NO/CO/O_2 reaction. Appl Catal B Environ 81:141–149. https://doi.org/10.1016/j.apcatb.2007.12.005
34. Luisetto I, Tuti S, Di Bartolomeo E (2012) Co and Ni supported on CeO_2 as selective bimetallic catalyst for dry reforming of methane. Int J Hydrog Energy 37:15992–15999. https://doi.org/10.1016/j.ijhydene.2012.08.006

35. Lucrédio AF, Assaf JM, Assaf EM (2011) Methane conversion reactions on Ni catalysts promoted with Rh: influence of support. Appl Catal A Gen 400:156–165. https://doi.org/10.1016/j.apcata.2011.04.035
36. Wu Chunfei C, Wang Leizhi L, Williams PT et al (2011) Hydrogen production from biomass gasification with Ni/MCM-41 catalysts: influence of Ni content. Appl Catal B Environ 108–109:6–13. https://doi.org/10.1016/j.apcatb.2011.07.023
37. Liu H, Wang H, Shen J et al (2008) Preparation, characterization and activities of the nano-sized Ni/SBA-15 catalyst for producing COx-free hydrogen from ammonia. Appl Catal A Gen 337:138–147. https://doi.org/10.1016/j.apcata.2007.12.006
38. Ren S, Zhang P, Shui H et al (2010) Promotion of Ni/SBA-15 catalyst for hydrogenation of naphthalene by pretreatment with ammonia/water vapour. Catal Commun 12:132–136. https://doi.org/10.1016/j.catcom.2010.08.022
39. Qiu S, Zhang X, Liu Q et al (2013) A simple method to prepare highly active and dispersed Ni/MCM-41 catalysts by co-impregnation. Catal Commun 42:73–78. https://doi.org/10.1016/j.catcom.2013.07.031
40. Ding C, Wang J, Ai G et al (2016) Partial oxidation of methane over silica supported Ni nanoparticles with size control by alkanol solvent. Fuel 175:1–12. https://doi.org/10.1016/j.fuel.2016.02.024
41. Wang SY, Li N, Zhou RM et al (2013) Comparing the CO oxidation activity of free PdO and Pd^{2+} ions over PdO-CeO_2/SiO_2 catalysts. J Mol Catal A Chem 374–375:53–58. https://doi.org/10.1016/j.molcata.2013.03.019
42. Ma Z, Meng X, Liu N, Shi L (2018) Pd-Ni doped sulfated zirconia: study of hydrogen spillover and isomerization of N-hexane. Mol Catal 449:114–121. https://doi.org/10.1016/j.mcat.2018.02.003
43. Montes De Correa C, Córdoba Castrillón F (2005) Supported bimetallic Pd-Co catalysts: characterization and catalytic activity. J Mol Catal A Chem 228:267–273. https://doi.org/10.1016/j.molcata.2004.09.033
44. Kumar N, Smith ML, Spivey JJ (2012) Characterization and testing of silica-supported cobalt-palladium catalysts for conversion of syngas to oxygenates. J Catal 289:218–226. https://doi.org/10.1016/j.jcat.2012.02.011
45. Stonkus V, Edolfa K, Leite L et al (2009) Palladium-promoted Co-SiO_2 catalysts for 1,4-butanediol cyclization. Appl Catal A Gen 362:147–154. https://doi.org/10.1016/j.apcata.2009.04.033
46. Jacobs G, Das TK, Patterson PM et al (2003) Fischer-Tropsch synthesis XAFS–XAFS studies of the effect of water on a Pt-promoted Co/Al_2O_3 catalyst. Appl Catal A Gen 247:335–343. https://doi.org/10.1016/S0926-860X(03)00107-8
47. Das TK, Jacobs G, Patterson PM et al (2003) Fischer-Tropsch synthesis: characterization and catalytic properties of rhenium promoted cobalt alumina catalysts. Fuel 82:805–815. https://doi.org/10.1016/S0016-2361(02)00361-7
48. Peck MA, Langell MA (2012) Comparison of nanoscaled and bulk NiO structural and environmental characteristics by XRD, XAFS, and XPS. Chem Mater 24:4483–4490. https://doi.org/10.1021/cm300739y
49. Larina TV, Dovlitova LS, Kaichev VV et al (2015) Influence of the surface layer of hydrated silicon on the stabilization of Co2+ cations in Zr-Si fiberglass materials according to XPS, UV-Vis DRS, and differential dissolution phase analysis. RSC Adv 5:79898–79905. https://doi.org/10.1039/c5ra12551k
50. Guo Z, Kang X, Zheng X et al (2019) PdCu alloy nanoparticles supported on CeO_2 nanorods: Enhanced electrocatalytic activity by synergy of compressive strain, PdO and oxygen vacancy. J Catal 374:101–109. https://doi.org/10.1016/j.jcat.2019.04.027
51. Post P, Wurlitzer L, Maus-Friedrichs W, Weber AP (2018) Characterization and applications of nanoparticles modified in-flight with silica or silica-organic coatings. Nanomaterials 8:1–19. https://doi.org/10.3390/nano8070530
52. Gostynski R, Fraser R, Landman M et al (2017) Synthesis and XPS characterization of Si-supported chromium(0) Fischer aminocarbene complexes. J Organomet Chem 836–837:62–67. https://doi.org/10.1016/j.jorganchem.2017.03.001
53. Abass MA, Syed AA, Gervais C, Singh G (2017) Synthesis and electrochemical performance of a polymer-derived silicon oxycarbide/boron nitride nanotube composite. RSC Adv 7:21576–21584. https://doi.org/10.1039/c7ra01545c
54. Zheng LL, Ma Q, Wang YH et al (2016) High-performance unannealed a-InGaZnO TFT with an atomic-layer-deposited SiO_2 insulator. IEEE Electron Device Lett 37:743–746. https://doi.org/10.1109/LED.2016.2558665
55. Li L, Tang D, Song Y et al (2018) Hydrogen production from ethanol steam reforming on Ni-Ce/MMT catalysts. Energy 149:937–943. https://doi.org/10.1016/j.energy.2018.02.116
56. Wang F, Zhang L, Zhu J et al (2018) Study on different CeO_2 structure stability during ethanol steam reforming reaction over Ir/CeO_2 nanocatalysts. Appl Catal A Gen 564:226–233. https://doi.org/10.1016/j.apcata.2018.07.036
57. Montero C, Oar-Arteta L, Remiro A et al (2015) Thermodynamic comparison between bio-oil and ethanol steam reforming. Int J Hydrog Energy 40:15963–15971. https://doi.org/10.1016/j.ijhydene.2015.09.125
58. da Silva AAA, Bion N, Epron F et al (2017) Effect of the type of ceria dopant on the performance of Ni/CeO_2 SOFC anode for ethanol internal reforming. Appl Catal B Environ 206:626–641. https://doi.org/10.1016/j.apcatb.2017.01.069
59. Augusto BL, Noronha FB, Fonseca FC et al (2014) Nickel/gadolinium-doped ceria anode for direct ethanol solid oxide fuel cell. Int J Hydrog Energy 39:11196–11209. https://doi.org/10.1016/j.ijhydene.2014.05.088
60. Nobrega SD, Gelin P, Georges S et al (2014) A fuel-flexible solid oxide fuel cell operating in gradual internal reforming. J Electrochem Soc 161:F354–F359. https://doi.org/10.1149/2.107403jes
61. Rodrigues TS, de Moura ABL, e Silva FA et al (2019) Ni supported Ce0.9Sm0.1O2-Δ nanowires: an efficient catalyst for ethanol steam reforming for hydrogen production. Fuel 237:1244–1253. https://doi.org/10.1016/j.fuel.2018.10.053
62. Wang F, Zhang L, Deng J et al (2019) Embedded Ni catalysts in Ni-O-Ce solid solution for stable hydrogen production from ethanol steam reforming reaction. Fuel Process Technol 193:94–101. https://doi.org/10.1016/j.fuproc.2019.05.004
63. Santander JA, Tonetto GM, Pedernera MN, López E (2017) Ni/CeO2–MgO catalysts supported on stainless steel plates for ethanol steam reforming. Int J Hydrog Energy 42:9482–9492. https://doi.org/10.1016/j.ijhydene.2017.03.169
64. Campos CH, Osorio-Vargas P, Flores-González N et al (2016) Effect of Ni loading on lanthanide (La and Ce) promoted γ-Al_2O_3 catalysts applied to ethanol steam reforming. Catal Lett 146:433–441. https://doi.org/10.1007/s10562-015-1649-6
65. Palma V, Ruocco C, Castaldo F et al (2015) Ethanol steam reforming over bimetallic coated ceramic foams: effect of reactor configuration and catalytic support. Int J Hydrog Energy 40:12650–12662. https://doi.org/10.1016/j.ijhydene.2015.07.138
66. Liu F, Qu Y, Yue Y et al (2015) Nano bimetallic alloy of Ni-Co obtained from LaCoxNi1-xO_3 and its catalytic performance for steam reforming of ethanol. RSC Adv 5:16837–16846. https://doi.org/10.1039/c4ra14131h
67. Ye JL, Wang YQ, Liu Y, Wang H (2008) Steam reforming of ethanol over Ni/CexTi1-xO_2 catalysts. Int J Hydrog Energy 33:6602–6611. https://doi.org/10.1016/j.ijhydene.2008.08.036
68. Zhang C, Hu X, Yu Z et al (2019) Steam reforming of acetic acid for hydrogen production over attapulgite and alumina supported Ni catalysts: Impacts of properties of supports on catalytic behaviors. Int J Hydrog Energy 44:5230–5244. https://doi.org/10.1016/j.ijhydene.2018.09.071

69. Sharma YC, Kumar A, Prasad R, Upadhyay SN (2017) Ethanol steam reforming for hydrogen production: Latest and effective catalyst modification strategies to minimize carbonaceous deactivation. Renew Sustain Energy Rev 74:89–103. https://doi.org/10.1016/j.rser.2017.02.049
70. Ogo S, Sekine Y (2020) Recent progress in ethanol steam reforming using non-noble transition metal catalysts: a review. Fuel Process Technol 199:106238. https://doi.org/10.1016/j.fuproc.2019.106238
71. Cheng F, Dupont V (2017) Steam reforming of bio-compounds with auto-reduced nickel catalyst. Catalysts 7:114. https://doi.org/10.3390/catal7040114
72. Song JH, Yoo S, Yoo J et al (2017) Hydrogen production by steam reforming of ethanol over Ni/Al_2O_3-La_2O_3 xerogel catalysts. Mol Catal 434:123–133. https://doi.org/10.1016/j.mcat.2017.03.009
73. Bussi J, Musso M, Quevedo A et al (2017) Structural and catalytic stability assessment of Ni-La-Sn ternary mixed oxides for hydrogen production by steam reforming of ethanol. Catal Today 296:154–162. https://doi.org/10.1016/j.cattod.2017.04.024
74. Shao J, Zeng G, Li Y (2017) Effect of Zn substitution to a $LaNiO_3-\Delta$perovskite structured catalyst in ethanol steam reforming. Int J Hydrog Energy 42:17362–17375. https://doi.org/10.1016/j.ijhydene.2017.04.066
75. Olivares ACV, Gomez MF, Barroso MN, Abello MC (2018) Ni-supported catalysts for ethanol steam reforming: effect of the solvent and metallic precursor in catalyst preparation. Int J Ind Chem 9:61–73. https://doi.org/10.1007/s40090-018-0135-6